Solar Phys (2016) 291:3385–3426
DOI 10.1007/s11207-016-0981-3

Spatio-temporal Dynamics of Sources of Hard X-Ray Pulsations in Solar Flares

S.A. Kuznetsov[1,2,3] · I.V. Zimovets[3,4,5,2] · A.S. Morgachev[1,2] · A.B. Struminsky[3,6] + R. Wang (NSSC/CAS)

Received: 14 February 2016 / Accepted: 20 August 2016 / Published online: 14 September 2016

On the importance of spatially-resolved observations of QPP sources

To select appropriate models!

[Zaitsev & Stepanov (AL, 1982)

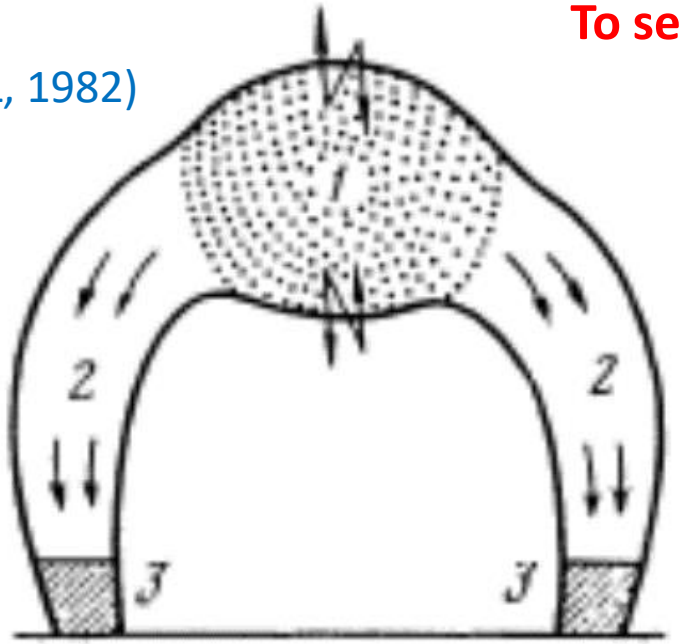

Vlahos (SSR, 1994)

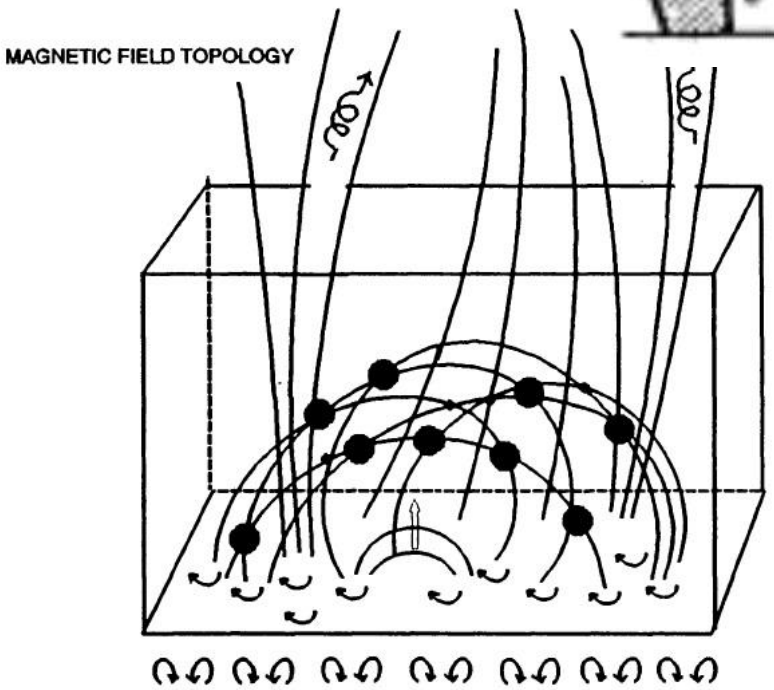

Adopted from
Priest & Forbes (AAR, 2002)

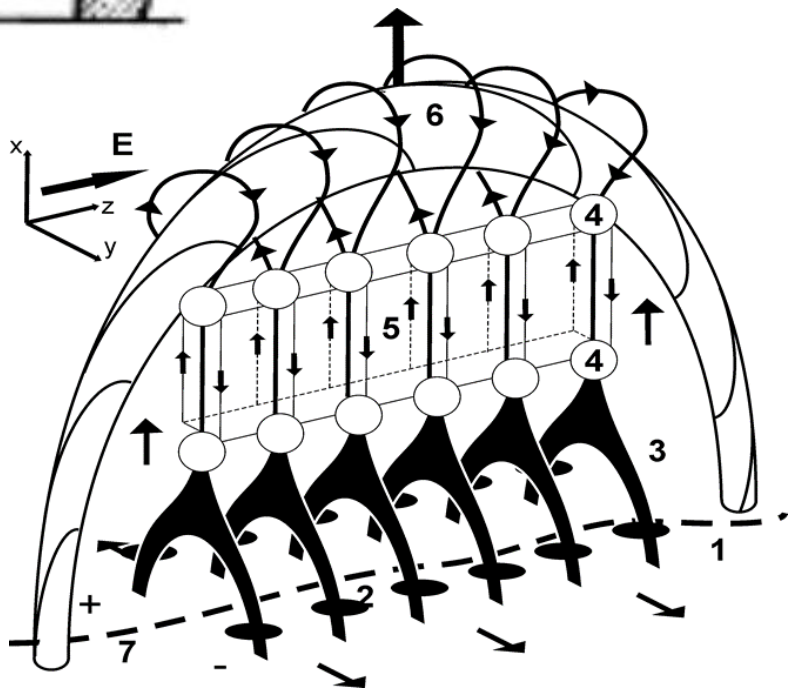

Dynamics of sources of HXR pulsations in flares: several case studies

- It is well known that HXR footpoint sources are not stationary in flares – they move, i.e. change their location in time [Sakao et al., 1998; Bogachev et al., ApJ, 2005; Yang et al., ApJ, 2009].
- This was found for several flares with QPPs of HXR emission and in a few flares with QPPs of microwave emission [Reznikova et al., ApJ, 2010; Kuznetsov et al., G&A, 2017, submitted].
- **No systematic analysis of flares with HXR pulsations was done before.**

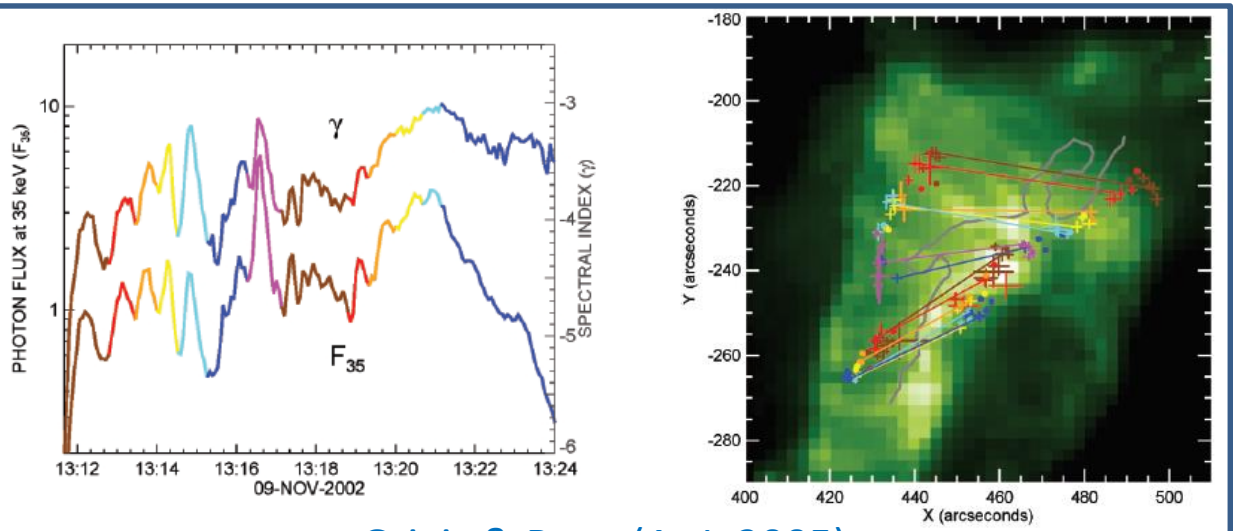

Grigis & Benz (ApJ, 2005)

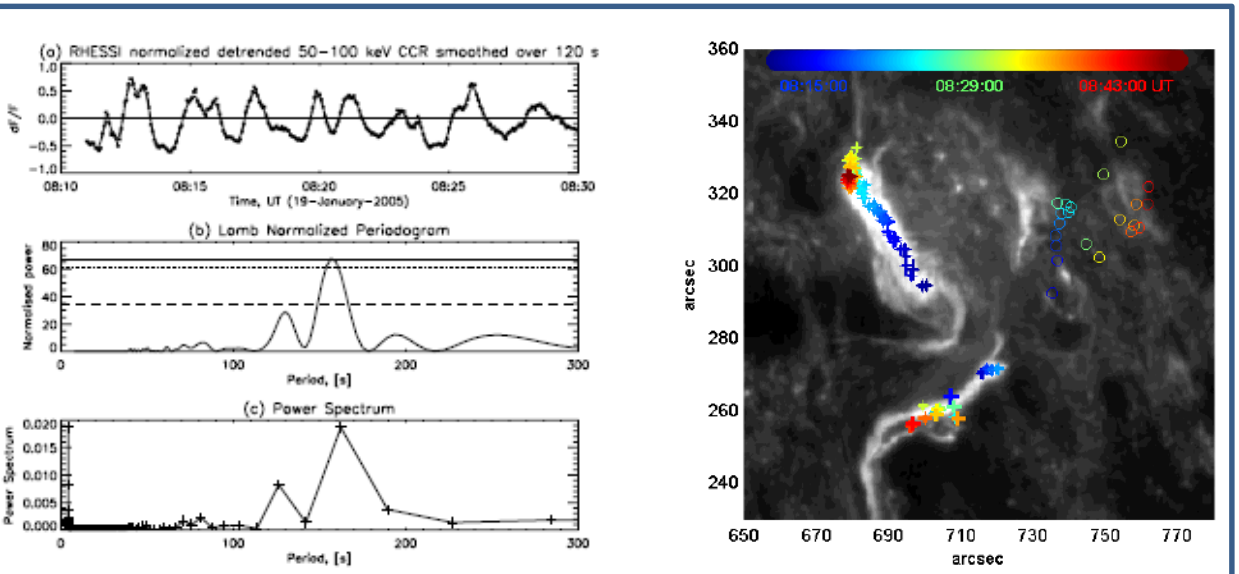

Zimovets & Struminsky (SoPh, 2009)

Generalization of case studies (<10) of HXR QPPs sources

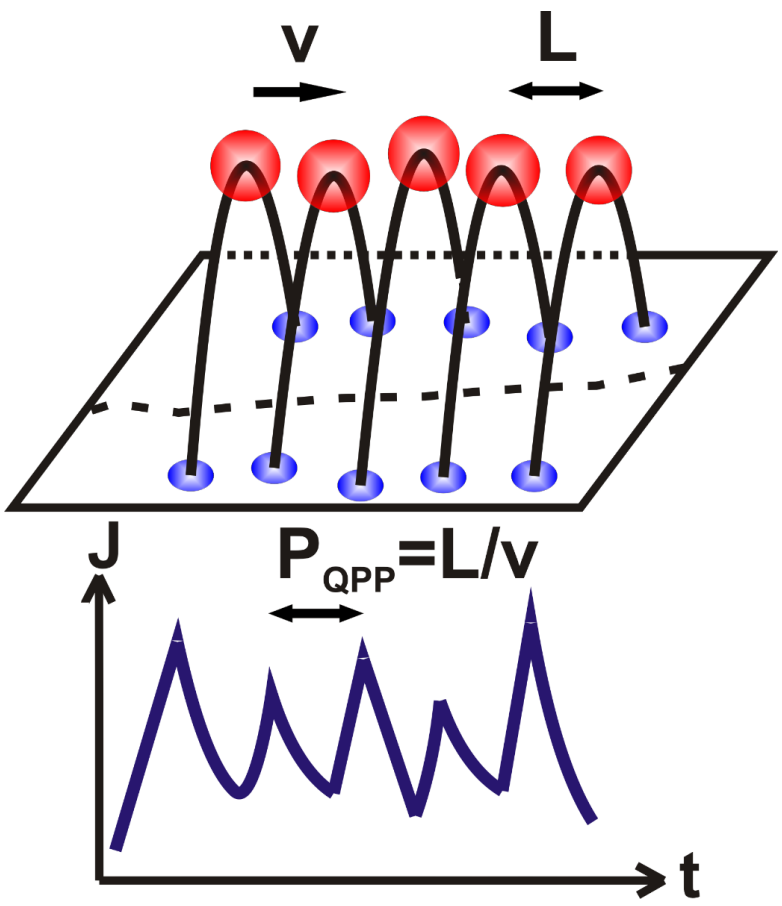

Zimovets (PhD, 2010)

Main Features:

- QPPs are not harmonic
- Different pulsations are emitted from different loops of flare arcades
- Primary energy release sites are (most probably) near the apex of flaring loops
- Energy release trigger propagates predominantly along flare arcade's axis and PIL
- V~10-100 km/s ($V < V_A$ & $V < V_S$)
- L~1000-10000 km
- **Single loop models don't satisfy these observations**

Aim of this research:

- Systematic analysis of spatio-temporal evolution (dynamics) of sources of HXR pulsations for a large sample of flares

Tasks of this research:

1. Flare selection from the RHESSI catalog
2. Selection of significant, real peaks of HXR pulsations
3. Image synthesis of HXR sources
4. Analysis of HXR sources dynamics (in respect to PILs)
5. Collection of additional information about selected flares
6. Generalization of observational results

Criteria of flare selection

- Existence of at least **4** successive peaks/pulsations in the RHESSI 50-100 keV energy channel (4-s resolution)
- Location of the flaring region near the disk center (selected 154 events)
- A signal-to-noise ratio in the 50-100 keV channel is sufficiently high to synthesize images
- A level of high-energy charged particles at the RHESSI detectors is low
- The RHESSI attenuators do not change too many times during a flare impulsive phase

29 events from 2002 to 2015.

1	2	3	4	5	6	7	8	9	10	11	12	13
Flare No	Date	RHESSI Flare No	GOES Start Time	GOES Peak Time	GOES End Time	GOES Class	NOAA AR No	Hale Class	RHESS Flare (arcsec)	Flare Group No	CME First Appear.	Radio Burst Types
1	14–Mar–02	2031402	01:38	01:50	02:02	M5.7	9866	bdg	-377, -76	1	No	III, IV
2	19–Aug–02	20819155	20:56	21:02	21:06	M3.1	10069	bdg	+487, -272	2	No	III
3	20–Aug–02	20820159	01:33	01:40	01:43	M5.0	10069	bdg	+533, -265	2	01:54	III
4	20–Aug–02	20820140	08:22	08:26	08:30	M3.4	10069	bdg	+569, -264	2	08:55	III, V
5	21–Aug–02	208211203	01:35	01:41	01:45	M1.4	10069	bdg	+693, -250	2	02:06	II, III
6	09–Nov–02	2110912	13:08	13:23	13:36	M4.6	10180	bdg	+432, -255	1	13:32	II, III, IV
7	29–May–03	30529100	00:51	01:05	01:12	X1.2	10365	bdg	+497, -106	1	01:27	II, III, IV
8	13–Jul–04	40713103	00:09	00:17	00:23	M6.7	10646	b	+656, +184	1	00:54	II, III
9	15–Jul–04	4071514	18:15	18:24	18:28	X1.6	10649	bdg	-648, -233	2	No	II
10	30–Oct–04	4103006	03:23	03:33	03:37	M3.3	10691	b	+319, +143	1	03:54	II, III
11	03–Nov–04	4110305	03:23	03:35	03:57	M1.6	10696	b	-679, +101	1	03:54	II, III, IV, V
12	04–Nov–04	4110460	22:53	23:09	23:26	M5.4	10696	bd	-283, +71	1	23:20	III, IV
13	06–Nov–04	4110630	00:11	00:34	00:42	M9.3	10696	bdg	-76, +88	1	01:32	II, III, IV
14	10–Nov–04	4111002	01:59	02:13	02:20	X2.5	10696	bdg	+710, +102	2	02:26	II, III, IV
15	01–Jan–05	5010148	00:01	00:31	00:39	X1.7	10715	bdg	-535, +125	1	00:54	II, III, IV
16	15–Jan–05	5011586	00:22	00:43	01:02	X1.2	10720	bd	-124, +294	2	No	IIIN
17	15–Jan–05	50115152	22:25	23:02	23:31	X2.6	10720	bd	+20, +310	1	23:07	II, III, IV
18	17–Jan–05	5011710	06:59	09:52	10:07	X3.8	10720	bd	+432, +305	1	09:54	II, III, IV
19	19–Jan–05	5011911	08:03	08:22	08:40	X1.3	10720	bg	+696, +314	1	08:30	II, III, IV
20	13–May–05	5051310	16:13	16:57	17:28	M8.0	10759	b	-174, +238	2	17:12	II, III, IV
21	10–Sep–05	5091026	21:30	22:11	22:43	X2.1	10808	bgd	-665, -254	2	21:52	II, III, IV
22	13–Sep–05	5091367	23:15	23:22	23:30	X1.7	10808	bgd	-24, -297	2	23:36	III, IV
23	15–Feb–11	11021565	01:44	01:56	02:06	X2.2	11158	bg	+205, -222	2	02:24	II, III, IV, V
24	07–Jun–11	11060702	06:16	06:41	06:59	M2.5	11226	b	+705, -353	1	06:49	II, III, IV
25	06–Sep–11	11090678	22:12	22:20	22:24	X2.1	11283	bd	+284, +131	1	23:06	II, III
26	18–Apr–14	14041818	12:31	13:03	13:20	M7.3	12036	bd	+499, -229	2	13:26	II, III, IV
27	22–Oct–14	14102243	14:02	14:28	14:50	X1.6	12192	bdg	-225, -317	1	16:16	III
28	24–Oct–14	14102478	21:07	21:41	22:13	X3.1	12192	bdg	+287, -329	2	21:48	No
29	09–Nov–14	14110936	15:24	15:32	15:38	M2.3	12205	bgd	-184, +188	1	No	III

Selection of the significant HXR peaks (pulsations)

1) Definition of the standard deviation $\sigma(F_{bgr})$ of pre-flare background in the RHESSI 50-100 keV corrected count rates (CCRs)
2) Identification of all local maxima and minima in the background-subtracted CCRs
3) Calculation of amplitudes for all peaks of CCRs
4) Selection of peaks, which satisfied condition: **Peak Level ≥ 3σ(F_{bgr})**
5) Definition of time differences **P** between all successive significant peaks, estimation averaged time differences **<P>**

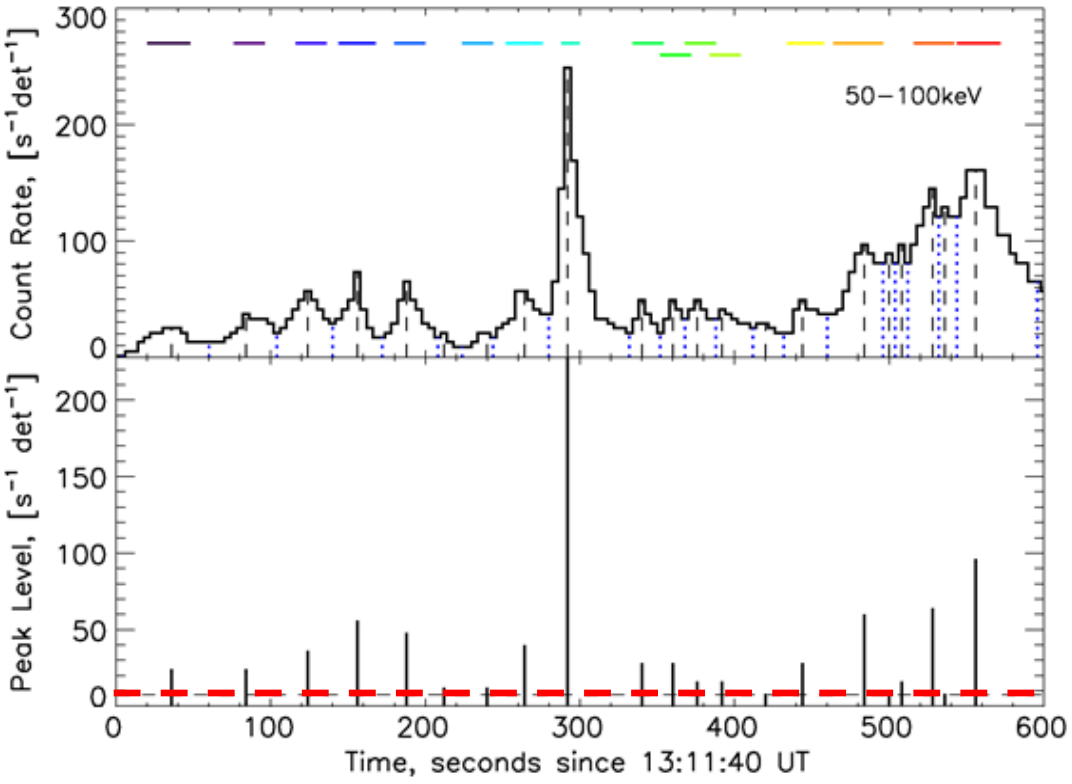

Horizontal colored lines indicate boundaries of time intervals for image synthesis

Table 2 Results of the analysis of the RHESSI background-subtracted corrected count rates in the 25 – 50 and 50 – 100 keV channels.

1	2	3	4	5	6	7	8	9	10	11	12	13	14	15
Flare no.	n_p	$\langle P \rangle$ [s]	σ_P [s]	N of peaks in $\langle P \rangle \pm 0.5\langle P \rangle$	N of peaks in $\langle P \rangle \pm 3.0\sigma_P$	n_p	$\langle P \rangle$ [s]	σ_P [s]	N of peaks in $\langle P \rangle \pm 0.5\langle P \rangle$	N of peaks in $\langle P \rangle \pm 3.0\sigma_P$	k_p	$\langle P' \rangle$ [s]	$\sigma(P')$ [s]	r_p
	25 – 50 keV channel					50 – 100 keV channel					50 – 100 keV channel			
1	27	22	13	19 (70 %)	26 (96 %)	25	28	25	10 (40 %)	24 (96 %)	10	61	35	2.5
2	5	19	12	2 (40 %)	5 (100 %)	5	23	10	3 (60 %)	5 (100 %)	5	23	10	1.0
3	15	20	11	8 (53 %)	15 (100 %)	9	26	18	5 (56 %)	9 (100 %)	7	25	13	1.3
4	9	21	12	6 (67 %)	9 (100 %)	9	17	6	7 (78 %)	9 (100 %)	5	22	4	1.8
5	10	21	7	8 (80 %)	10 (100 %)	9	26	21	6 (67 %)	9 (100 %)	5	18	4	1.8
6	21	27	13	16 (76 %)	21 (100 %)	21	26	12	14 (67 %)	21 (100 %)	16	36	13	1.3
7	18	28	15	7 (39 %)	18 (100 %)	13	31	17	7 (54 %)	13 (100 %)	6	70	7	2.2
8	15	16	5	13 (87 %)	15 (100 %)	13	19	5	13 (100 %)	13 (100 %)	11	21	11	1.2
9	7	17	7	7 (100 %)	7 (100 %)	7	20	7	7 (100 %)	7 (100 %)	5	23	2	1.4
10	14	22	12	8 (57 %)	14 (100 %)	13	22	11	8 (62 %)	13 (100 %)	8	34	13	1.6
11	15	19	7	13 (87 %)	15 (100 %)	12	20	9	8 (67 %)	12 (100 %)	6	30	12	2.0
12	36	24	26	19 (53 %)	36 (100 %)	19	40	31	12 (63 %)	18 (95 %)	8	46	28	2.4
13	6	43	23	3 (50 %)	6 (100 %)	9	30	22	6 (67 %)	9 (100 %)	7	39	22	1.3
14	31	19	10	17 (55 %)	31 (100 %)	13	44	22	10 (77 %)	12 (92 %)	8	47	10	1.6
15	12	22	14	9 (75 %)	12 (100 %)	7	19	9	3 (43 %)	7 (100 %)	5	22	10	1.4
16	10	19	11	5 (50 %)	10 (100 %)	9	23	12	9 (56 %)	9 (100 %)	8	30	6	1.1
17	54	39	44	27 (50 %)	54 (100 %)	103	22	19	87 (84 %)	100 (97 %)	15	86	25	6.9
18	36	22	15	27 (75 %)	35 (97 %)	32	25	18	18 (56 %)	32 (100 %)	13	55	37	2.5
19	55	20	15	46 (84 %)	54 (98 %)	18	60	46	8 (44 %)	18 (100 %)	11	87	47	1.6
20	20	21	9	16 (80 %)	20 (100 %)	14	33	34	6 (43 %)	14 (100 %)	6	86	25	2.3
21	103	23	25	65 (63 %)	102 (99 %)	89	31	34	44 (49 %)	87 (98 %)	12	133	30	7.4
22	6	27	30	1 (17 %)	6 (100 %)	13	33	34	6 (46 %)	13 (100 %)	6	22	12	2.2
23	35	16	7	31 (89 %)	35 (100 %)	29	20	9	20 (69 %)	29 (100 %)	12	33	7	2.4
24	36	26	14	21 (58 %)	36 (100 %)	41	23	14	29 (71 %)	40 (98 %)	13	51	11	3.2
25	20	21	14	13 (65 %)	20 (100 %)	10	28	21	3 (33 %)	10 (100 %)	8	23	8	1.3
26	23	24	16	15 (65 %)	23 (100 %)	30	20	13	18 (60 %)	29 (97 %)	11	48	35	2.7
27	10	21	10	5 (50 %)	10 (100 %)	6	35	10	6 (100 %)	6 (100 %)	5	30	6	1.2
28	34	17	8	22 (65 %)	34 (100 %)	15	27	18	11 (73 %)	15 (100 %)	9	44	17	1.7
29	8	20	12	4 (50 %)	8 (100 %)	7	19	5	7 (100 %)	7 (100 %)	7	26	8	1.0

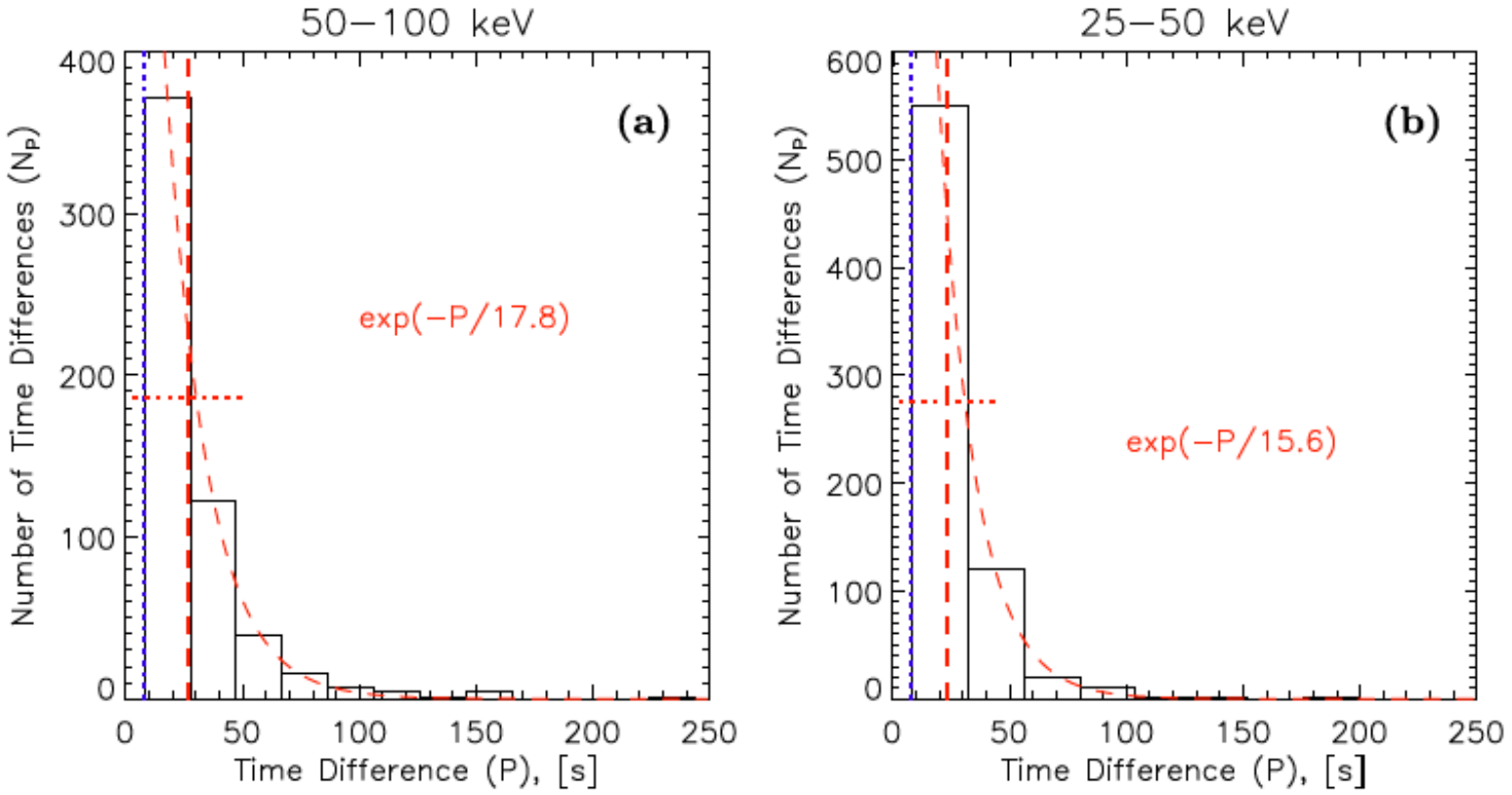

Figure 3 Combined distributions of the time differences (P) found in the four-second RHESSI background–subtracted corrected count rates in the 50 – 100 keV (a) and 25 – 50 keV (b) channels for all 29 studied flares. The red vertical dashed line shows the averaged time difference. The red horizontal dotted line shows the standard deviation of time differences at half the maxima of the distributions. The blue vertical dotted line shows the lower threshold ($P_{\rm thr} = 8$ s) of time differences, which can be found in the four-second count rates. The red thin dashed curves show Gaussian functions found by the best fit of the distributions.

Definition of HXR sources locations

- Identification of the HXR sources S^+ and S^- as centroids of contours at 30% peak-level on the HXR images
- Overlaying contours of the HXR sources S^+ (positive polarity) and S^- (negative polarity) on the MDI/HMI magnetograms
- Different colors of contours correspond to different significant HXR peaks

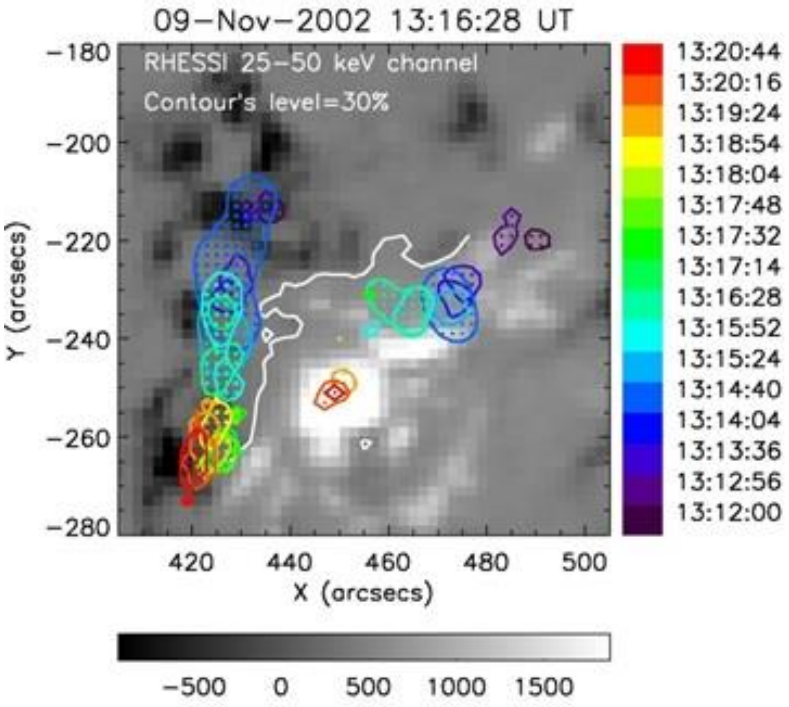

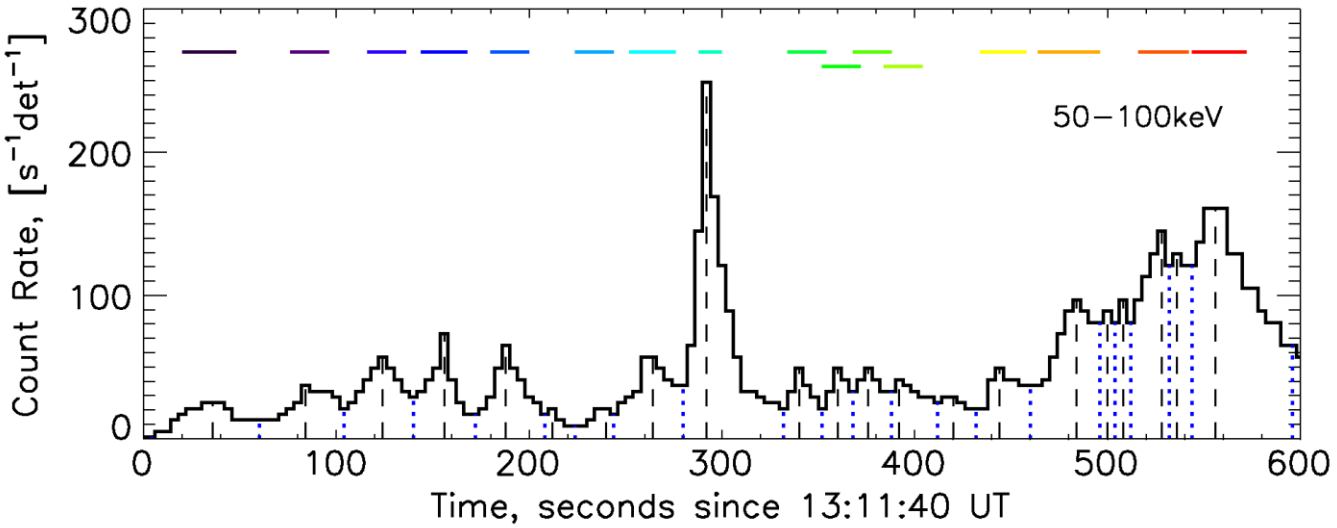

Separation of flares into 2 groups

Group-1

SOHO/MDI 09-Nov-2002 13:16:28 UT

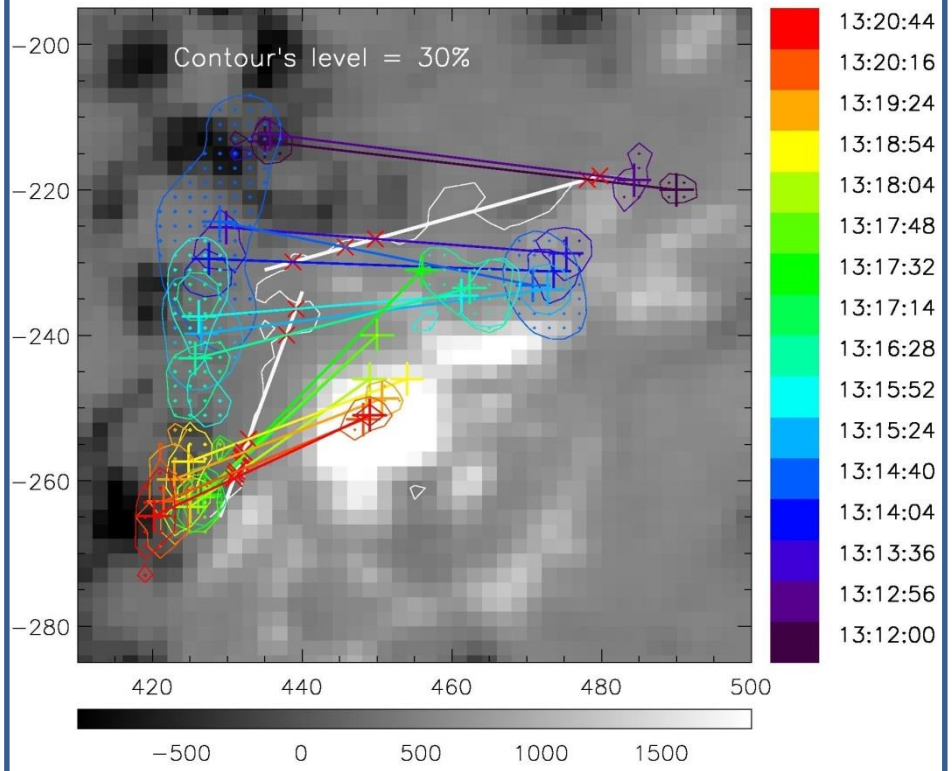

- **16** events (**55%**, two-ribbon flares)
- HXR sources are located in regions of different magnetic polarities
- Paired HXR sources move mainly along PIL with simple elongated shape

Group-2

SOHO/MDI 20-Aug-2002 08:25:32 UT

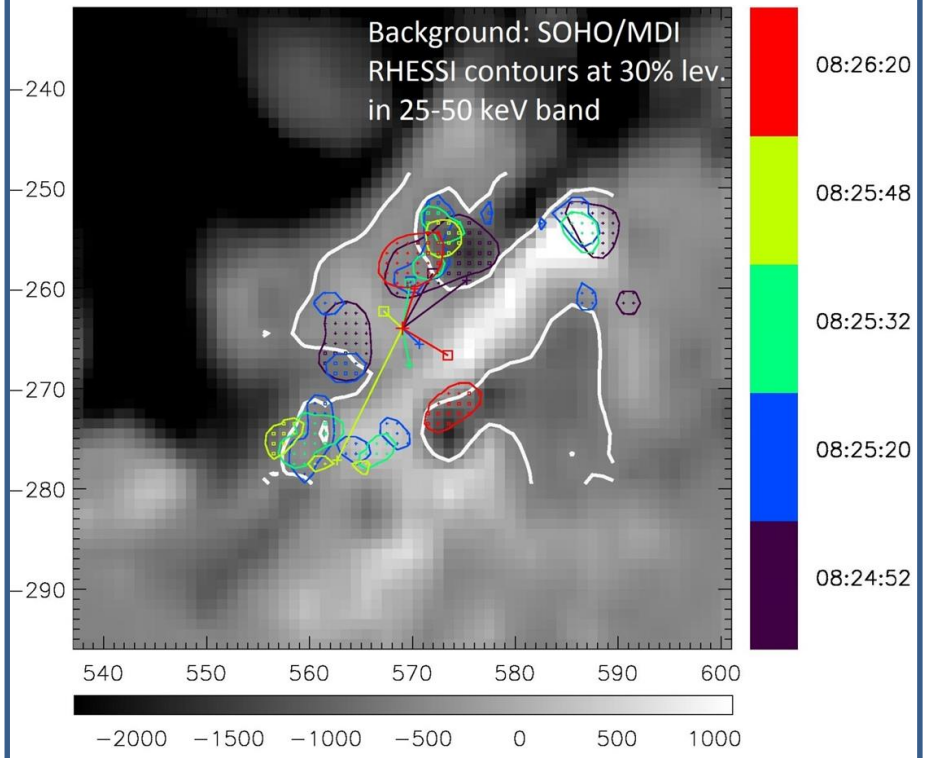

- **13** events (**45%** of all events)
- Random dynamics of HXR sources
- Presence of several PILs of complicated shape in a parent AR

Parameters of dynamics of HXR sources (for group-1 only)

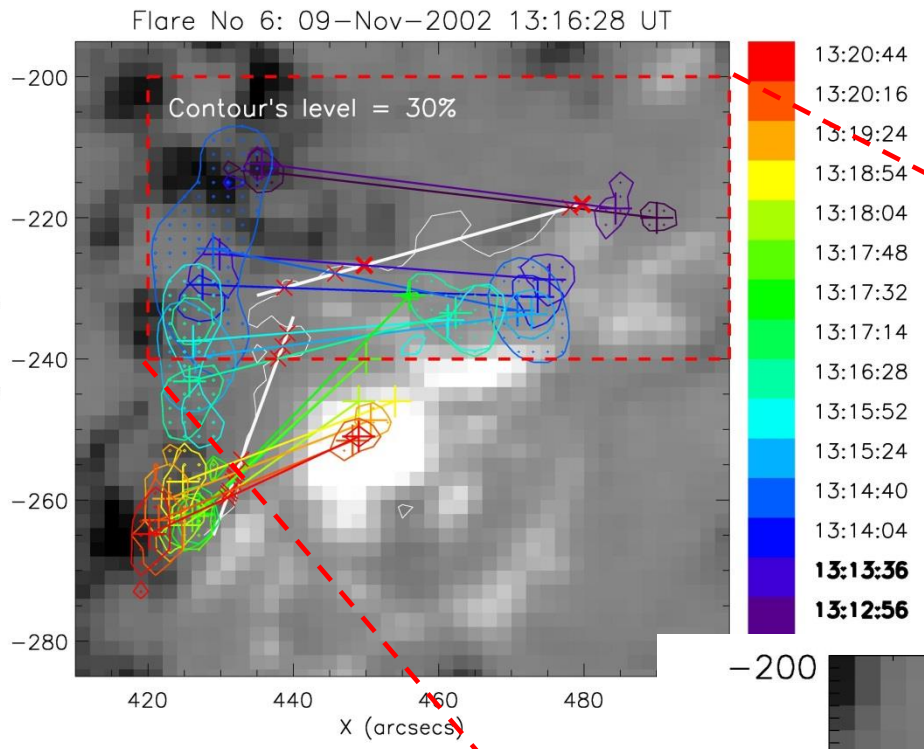

D_s – distance between sources S^+ и S^-

D_{IP} – distance between IP at two successive HXR peaks

$V_{IP} = D_{IP} / \Delta T$ – velocity of displacement of the IP between two successive HXR peaks

Zoom of active region

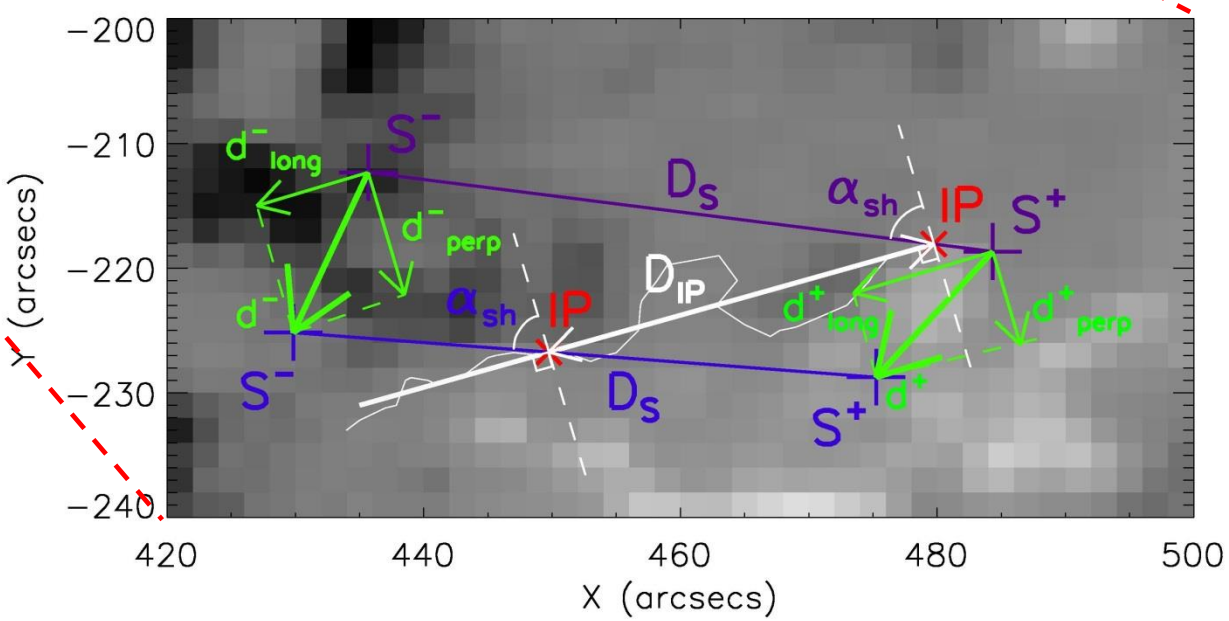

IP – intersection point between a line segment connecting S^+ and S^- sources and a PIL

Time profiles of the parameters of the HXR pulsations sources

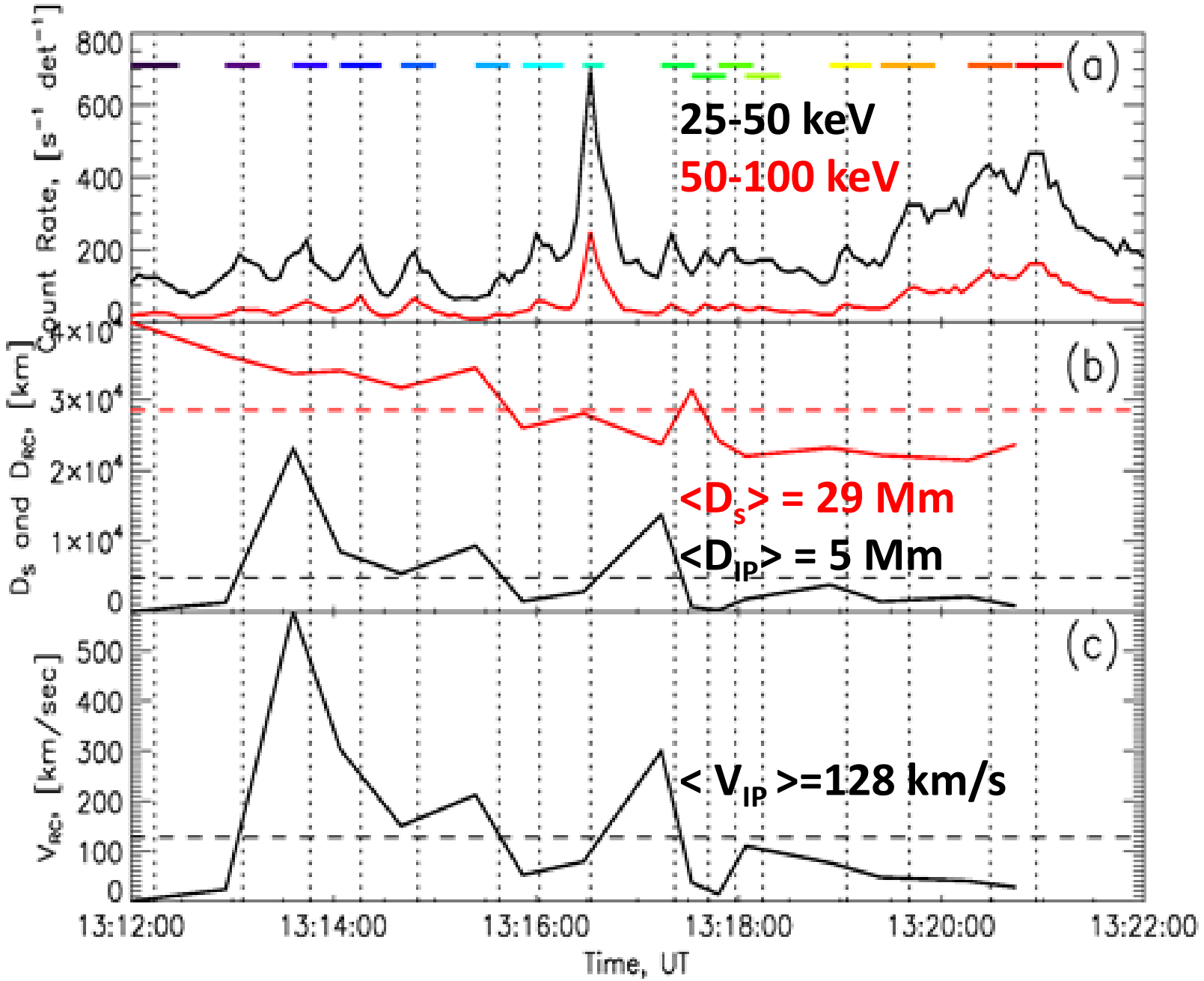

Quantitative parameters of sources of HXR pulsations for the group-1 events

1	2	3	4	5	6	7	8	9	10	11	12	13	14	15	16
Flare No	$\langle D_S \rangle$, [Mm]	$\sigma(D_S)$, [Mm]	$\langle \alpha_{sh} \rangle$, [Deg]	$\sigma(\alpha_{sh})$, [Deg]	$\langle D_{RC} \rangle$, [km]	$\sigma(D_{RC})$, [km]	$\langle v_{RC} \rangle$, [km/s]	$\sigma(v_{RC})$, [km/s]	$\langle v^+ \rangle$, [km/s]	$\sigma(v^+)$, [km/s]	$\langle v^- \rangle$, [km/s]	$\sigma(v^-)$, [km/s]	R^+	R^-	Types of Dynamics
1	24	8	40	17	1600	1460	36	36	57	61	57	63	2.4	0.6	A+D+C
6	29	6	53	16	4767	6236	128	154	160	156	105	93	1.8	3.8	A+D
7	16	4	32	15	965	860	14	12	56	93	90	66	1.3	1.8	A+C
8	10	4	28	18	2932	7876	120	301	71	52	61	91	1.3	1.1	A+B+C
10	13	4	48	16	1612	1440	51	50	53	48	37	49	1.4	2.1	A
11	22	4	40	6	1570	1485	61	51	110	87	81	89	3.5	1.0	A
12	40	1	61	3	1931	1630	23	17	28	31	18	20	0.9	1.4	A
13	22	1	20	5	1177	1024	40	42	48	42	50	65	3.2	3.2	A+C
15	17	2	5	7	723	989	27	41	72	50	46	45	0.8	1.8	A+D+C
17	30	6	52	21	6680	8550	50	51	64	57	50	94	3.1	1.7	A+C
18	26	10	31	14	1146	1113	44	64	107	132	73	76	1.0	1.6	A+C
19	36	10	1	8	5046	3890	72	63	70	59	35	26	4.9	0.3	A+B+C
24	18	4	31	10	1395	1170	24	23	48	54	32	23	4.4	6.0	A+C
25	9	4	37	17	1843	2100	61	60	86	106	103	155	1.6	0.8	A+C
27	42	6	34	5	1546	2212	38	50	67	68	88	101	3.5	1.1	A+D
29	11	3	72	4	1060	1161	59	66	63	46	97	71	5.3	4.9	A

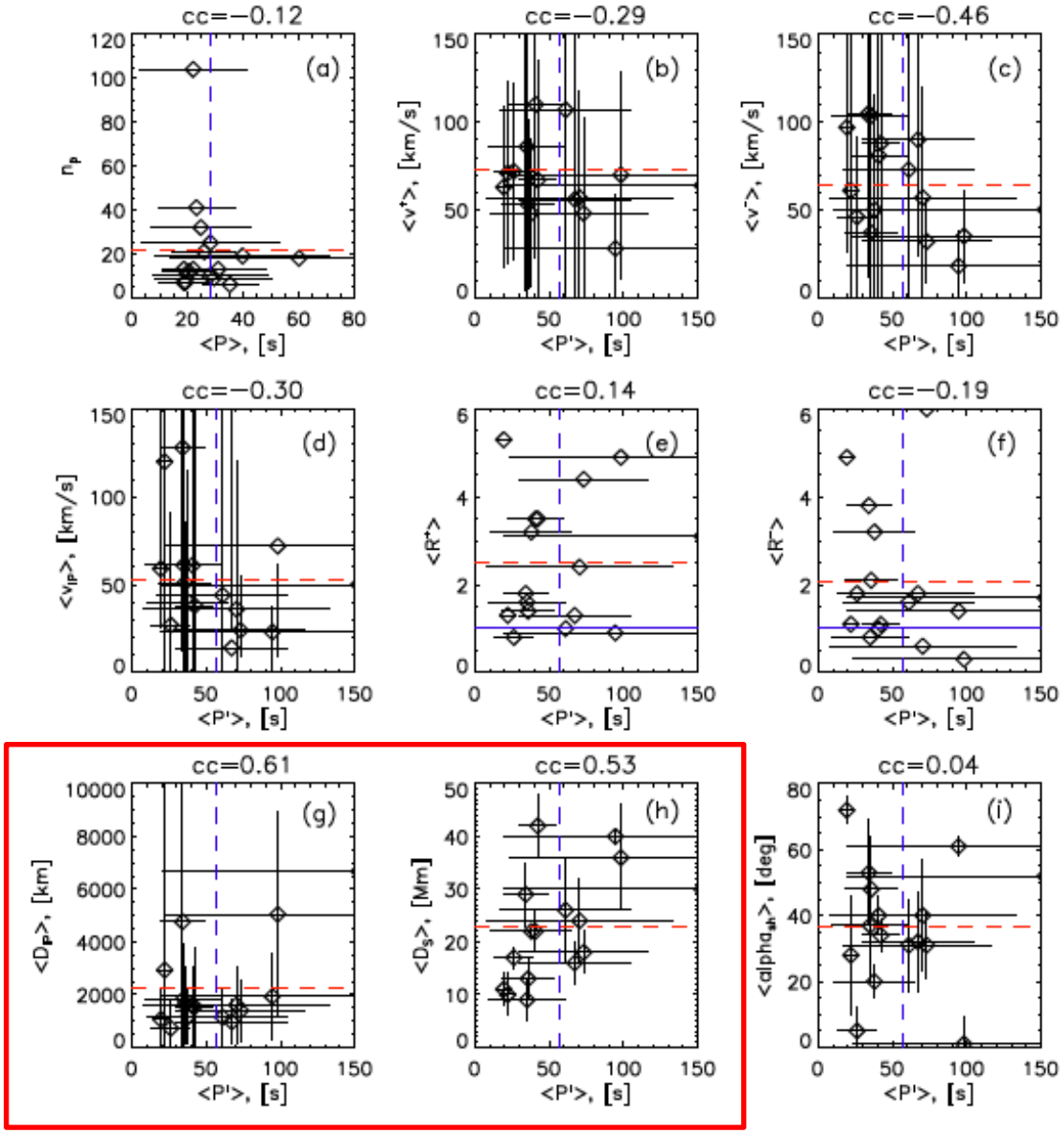

Figure 8 Mean quantitative characteristics of the dynamics of the paired HXR pulsation sources calculated for group 1 flares (diamonds). Errors (standard deviations; see Table 4) are shown by black thin solid horizontal and vertical segments. The mean values of the characteristics, averaged over all flares, are shown by red horizontal and blue vertical dashed lines. The blue horizontal solid lines in panels (e) and (f) show the level of 1. The linear Pearson correlation coefficient (*cc*) calculated for each pair of the variables is shown at the top.

Interesting correlations found

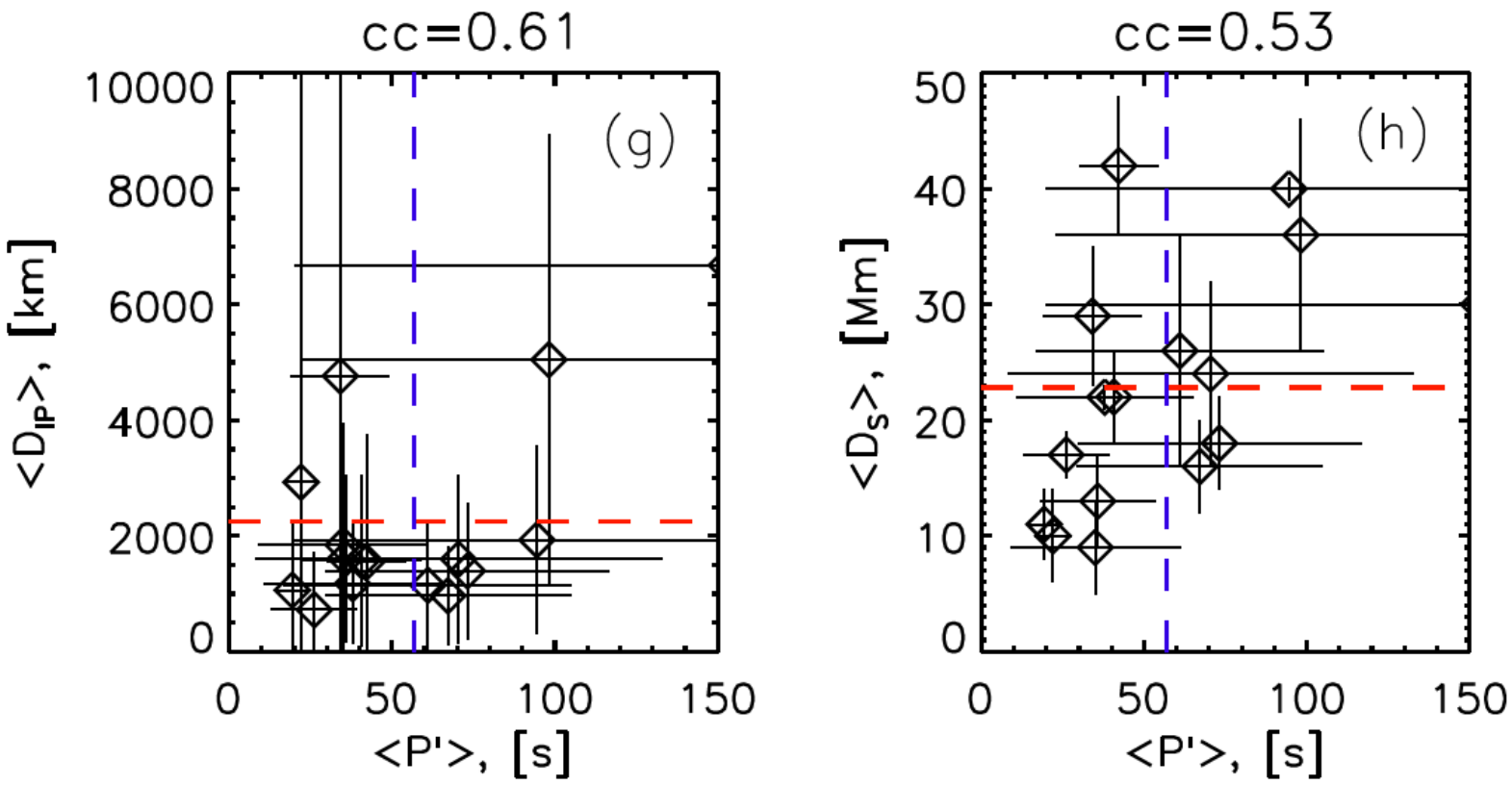

D_{IP} – distance between IPs at two successive HXR pulsations

D_s – distance between paired HXR sources S^+ и S^- (≈ loop length)

P' – corrected time difference between two successive HXR pulsations

Possibly, the most interesting observational result

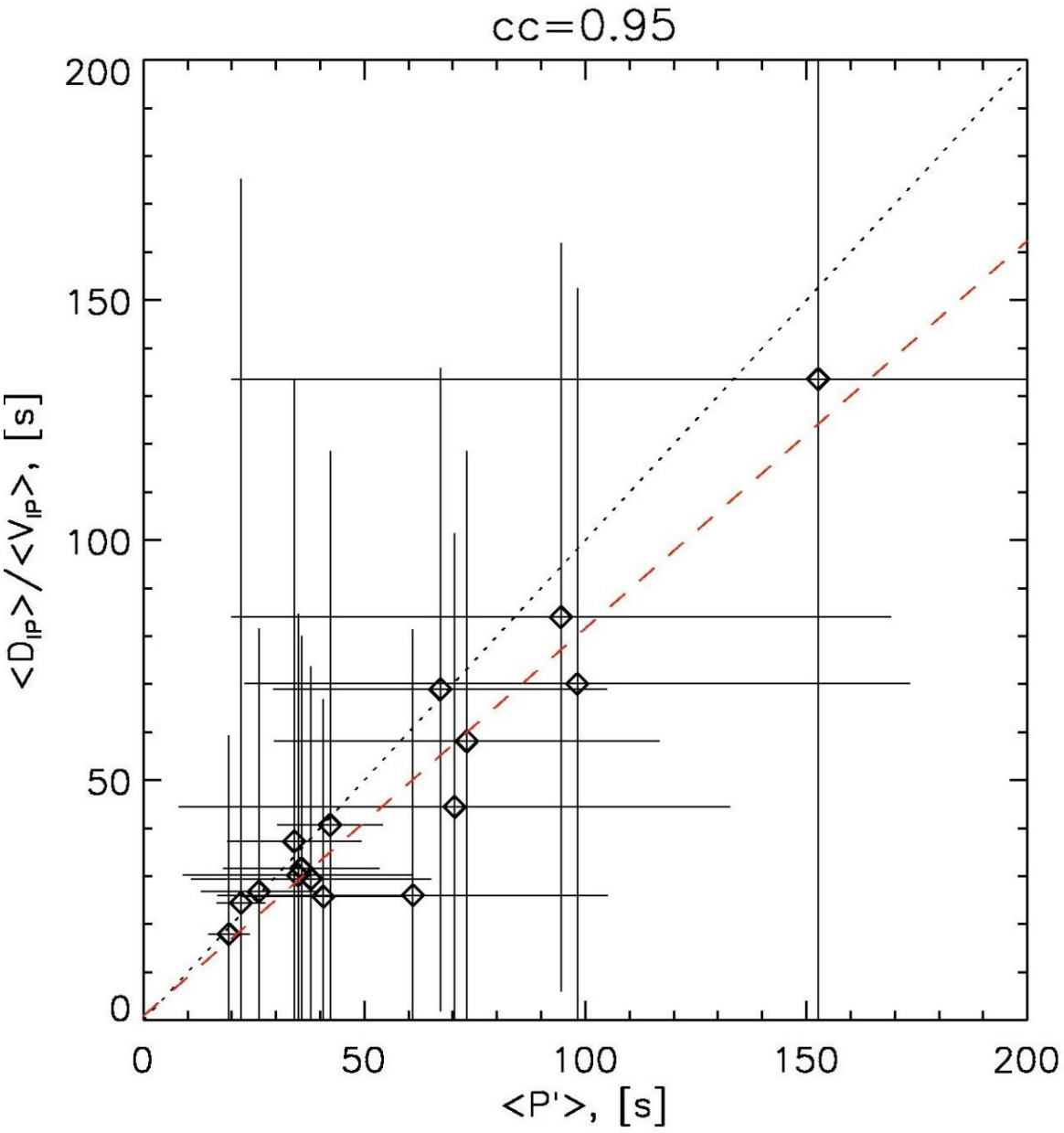

1	2	3	4	5	6	7	8	9	10	11	12	13
Flare No	Date	RHESSI Flare No	GOES Start Time	GOES Peak Time	GOES End Time	GOES Class	NOAA AR No	Hale Class	RHESS Flare (arcsec)	Flare Group No	CME First Appear.	Radio Burst Types
21	10–Sep–05	5091026	21:30	22:11	22:43	X2.1	10808	bgd	-665, -254	2	21:52	II, III, IV
22	13–Sep–05	5091367	23:15	23:22	23:30	X1.7	10808	bgd	-24, -297	2	23:36	III, IV
23	15–Feb–11	11021565	01:44	01:56	02:06	X2.2	11158	bg	+205, -222	2	02:24	II, III, IV, V
24	07–Jun–11	11060702	06:16	06:41	06:59	M2.5	11226	b	+705, -353	1	06:49	II, III, IV
25	06–Sep–11	11090678	22:12	22:20	22:24	X2.1	11283	bd	+284, +131	1	23:06	II, III
26	18–Apr–14	14041818	12:31	13:03	13:20	M7.3	12036	bd	+499, -229	2	13:26	II, III, IV
27	22–Oct–14	14102243	14:02	14:28	14:50	X1.6	12192	bdg	-225, -317	1	16:16	III
28	24–Oct–14	14102478	21:07	21:41	22:13	X3.1	12192	bdg	+287, -329	2	21:48	No
29	09–Nov–14	14110936	15:24	15:32	15:38	M2.3	12205	bgd	-184, +188	1	No	III

- **More than 85% of the flares studied were associated with CMEs, i.e. were eruptive events**
- **93% of the flares studied were associated with type III radio bursts – an evidence of escaping energetic electrons from flare regions (via reconnection?)**
- **6 out of 7 flares in the SDO epoch (after 2010) were accompanied by low coronal eruptions/ejections (LCEs) observed by AIA/SDO in the EUV range**
- **NLFFF reconstructions with HMI/SDO vector magnetograms show the presence of flux-ropes prior to all these 7 flares**

Examples of the NLFFF reconstructions for the SDO epoch flares

(Thanks to Dr. R. Wang, NSSC/CAS)

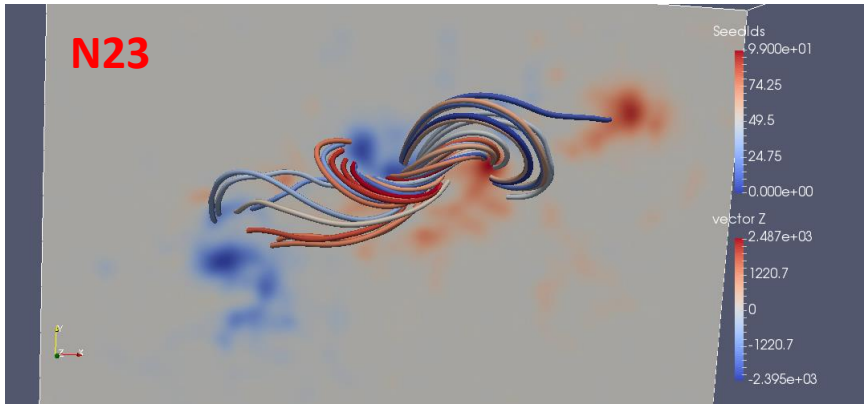

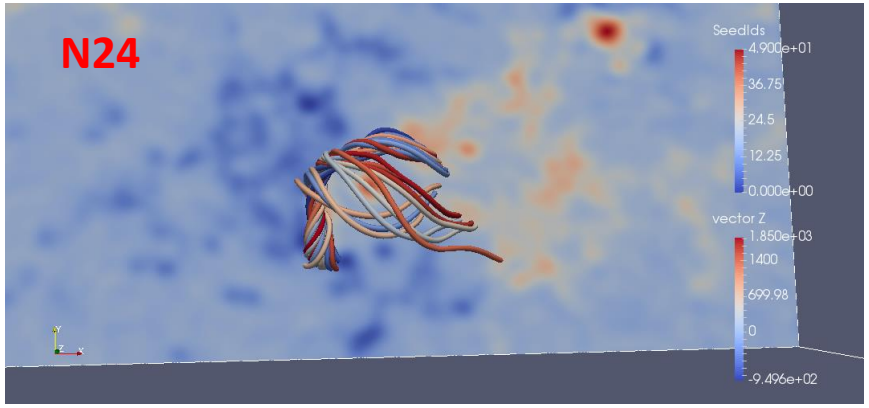

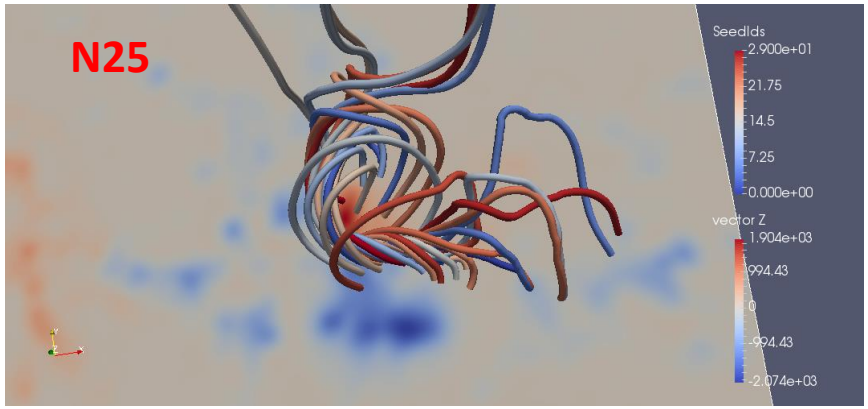

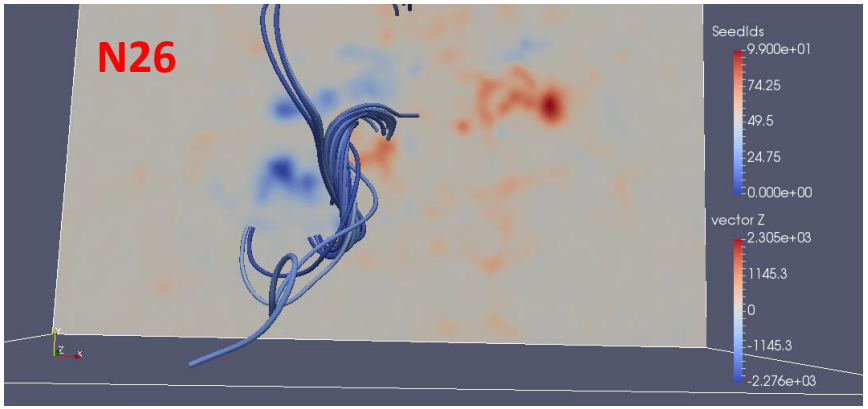

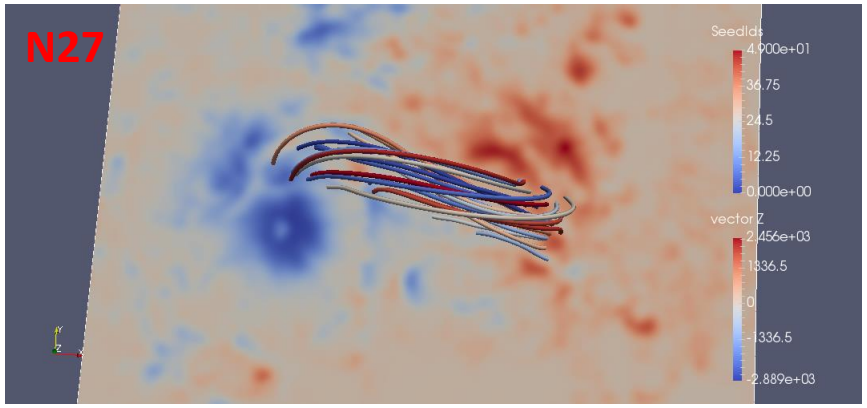

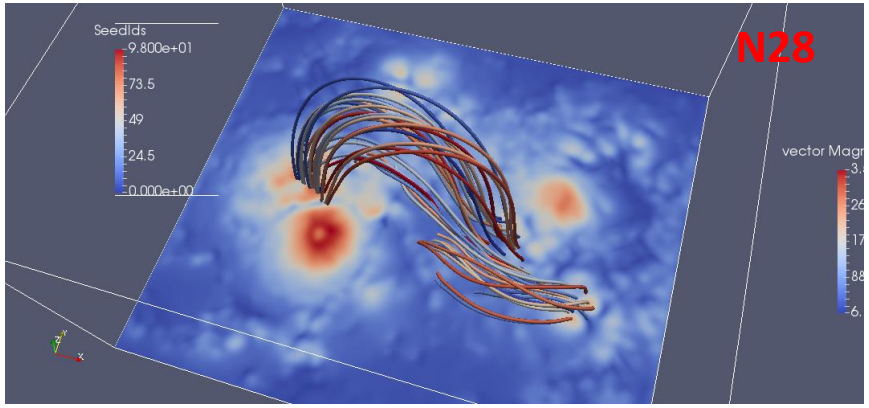

Working hypothesis:

Erupting flux-rope as a possible trigger of energy release in multiple coronal loops systems

"Elementary flare bursts" & HXR pulsations are resulted from successive interactions of different flux-rope parts with different surrounding loops

Group-1 flare

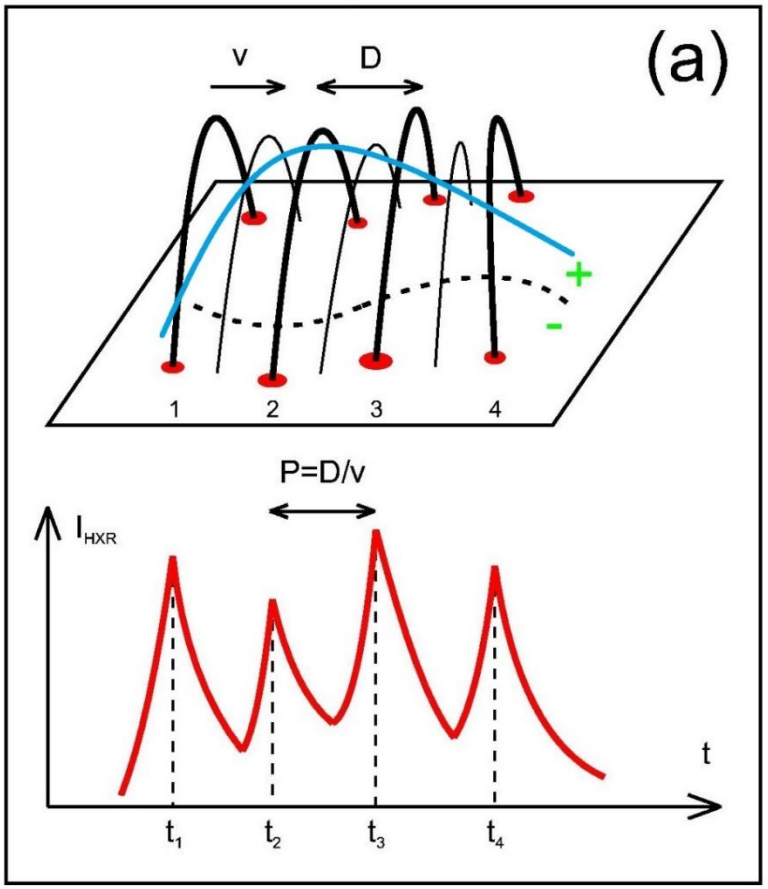

Two-ribbon flares

Group-2 flare

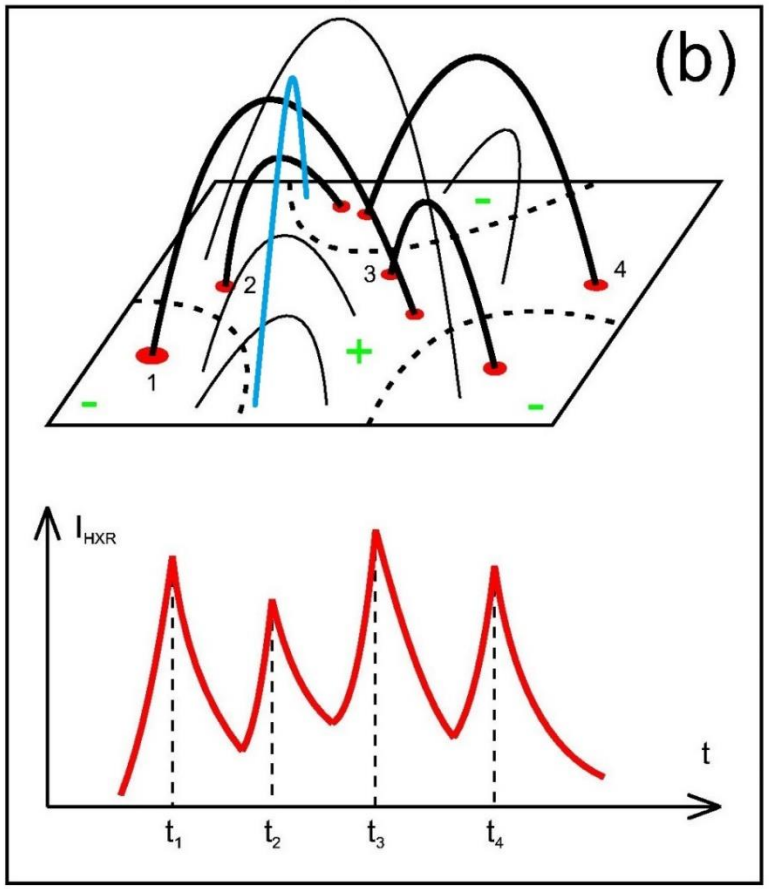

Complex magnetic topology

Conclusions

- **For the first time the systematic analysis of the dynamics of sources of HXR (25-100 keV) pulsations in a large sample of solar flares (2002-2015) is done**

- **It is shown that the location of the sources of HXR pulsations is not stationary: the sources move from pulsation to pulsation in all the flares studied**

- **The single-loop models do not satisfy these observations**

- **Displacement of the HXR sources from pulsation to pulsation can be interpreted by successive interaction of different parts of an erupting magnetic flux-rope with different surround magnetic flux tubes (loops)**

- **What is the reason for the quasi-periodicity (and whether it is significant/real) of HXR pulsations is still an interesting question**

Possible continuation of this study

- Implementing new techniques of time-series analysis (EMD, etc.) to all flares from our catalogue
- More deep analysis of the NLFFF-reconstructed magnetic configuration for all available flares + analysis of electric currents
- More deep and broad analysis of EUV images/movies for all possible flares from the catalogue
- Analysis of the HXR source dynamics relative to reconstructed magnetic fields
- **Suggestions are welcomed!**

Some new knowledge on flare energy release & QPPs?

Thank you for attention!

Bon Appetit!